1 **Title**

2 Unexpected enzyme-catalysed [4+2] cycloaddition and rearrangement in polyether

3 antibiotic biosynthesis

4

5 **Authors:**

6 Rory Little[1], Fernanda C. R. Paiva[2], Rob Jenkins[3], Hui Hong[1], Yuhui Sun[4], Yuliya

7 Demydchuk[1‡], Markiyan Samborskyy[1], Manuela Tosin[3], Finian J. Leeper[5], Marcio V.

8 B. Dias[2,3], Peter F. Leadlay [1]*.

9
10 **Affiliations:**
11
12 [1]Department of Biochemistry, University of Cambridge, 80 Tennis Court Road, CB2
13 1GA Cambridge, United Kingdom.
14
15 [2]Department of Microbiology, Institute of Biomedical Sciences II, University of São
16 Paulo, Avenida Professor Lineu Prestes, 1374 São Paulo, Brazil.
17
18 [3]Department of Chemistry, University of Warwick, Gibbet Hill, CV4 7AL Coventry,
19 United Kingdom.
20
21 [4]Key Laboratory of Combinatorial Biosynthesis and Drug Discovery, Ministry of
22 Education, School of Pharmaceutical Sciences, Wuhan University, 430071 Wuhan,
23 People's Republic of China.
24
25 [5]Department of Chemistry, University of Cambridge, Lensfield Road, CB2 1EW
26 Cambidge, United Kingdom.
27
28 ‡Current address: Bicycle Therapeutics Limited B900, Babraham Research Campus,
29 CB22 3AT Cambridge, United Kingdom
30
31 *Corresponding author. Email: pfl10@cam.ac.uk
32

33

34

35

36

37   **Abstract**

38

39   Enzymes catalysing remarkable Diels-Alder-like [4+2] cyclisations have been

40   previously implicated in the biosynthesis of spirotetronate and spirotetramate

41   antibiotics. Biosynthesis of the polyether antibiotic tetronasin is not anticipated to

42   require such steps, yet the tetronasin gene cluster encodes enzymes Tsn11 and Tsn15,

43   homologous to authentic [4+2] cyclases. Here we show that deletion of Tsn11 led to

44   accumulation of a late-stage intermediate, in which the two central rings of tetronasin,

45   and four of its 12 asymmetric centres, remain unformed. *In vitro* reconstitution

46   showed that Tsn11 catalyses an apparent inverse-electron-demand hetero Diels-Alder-

47   like [4+2] cyclisation of this species to an unexpected oxadecalin compound, which is

48   then rearranged by Tsn15 to form tetronasin. To gain structural and mechanistic

49   insight into the activity of Tsn15, a 1.7 Å crystal structure of a Tsn15-substrate

50   complex has been solved.

51

52   **Introduction**

53   The Diels-Alder reaction[1], in which a 1,3-diene and an alkene (dienophile) undergo a

54   concerted [4+2] cycloaddition to form a cyclohexene ring, is of central importance to

55   synthetic organic chemistry[2]. Transformations during the biosynthesis of numerous

56   cyclic microbial metabolites have been speculated to be catalysed by naturally-

57   evolved [4+2] cyclase ("Diels-Alderase") enzymes[3,4], and several enzymes have been

58   shown to catalyse [4+2] cyclisations consistent with this mechanism[5–12]. Almost all

59   examples studied so far involve the combination of an electron-rich 1,3-diene with an

60   electron-poor dienophile to form cyclohexene-containing products. Important

61   exceptions are the hetero-[4+2] cycloadditions catalysed by the pyridine synthases of

62 thiopeptide antibiotic biosynthesis[13] and by LepI, which installs a dihydropyran

63 during leporin B biosynthesis[14] (Fig. 1a). In the case of LepI, an electron-poor

64 (oxygen-based) diene reacts with an electron-rich dienophile in an inverse-electron-

65 demand hetero-Diels–Alder reaction[14].
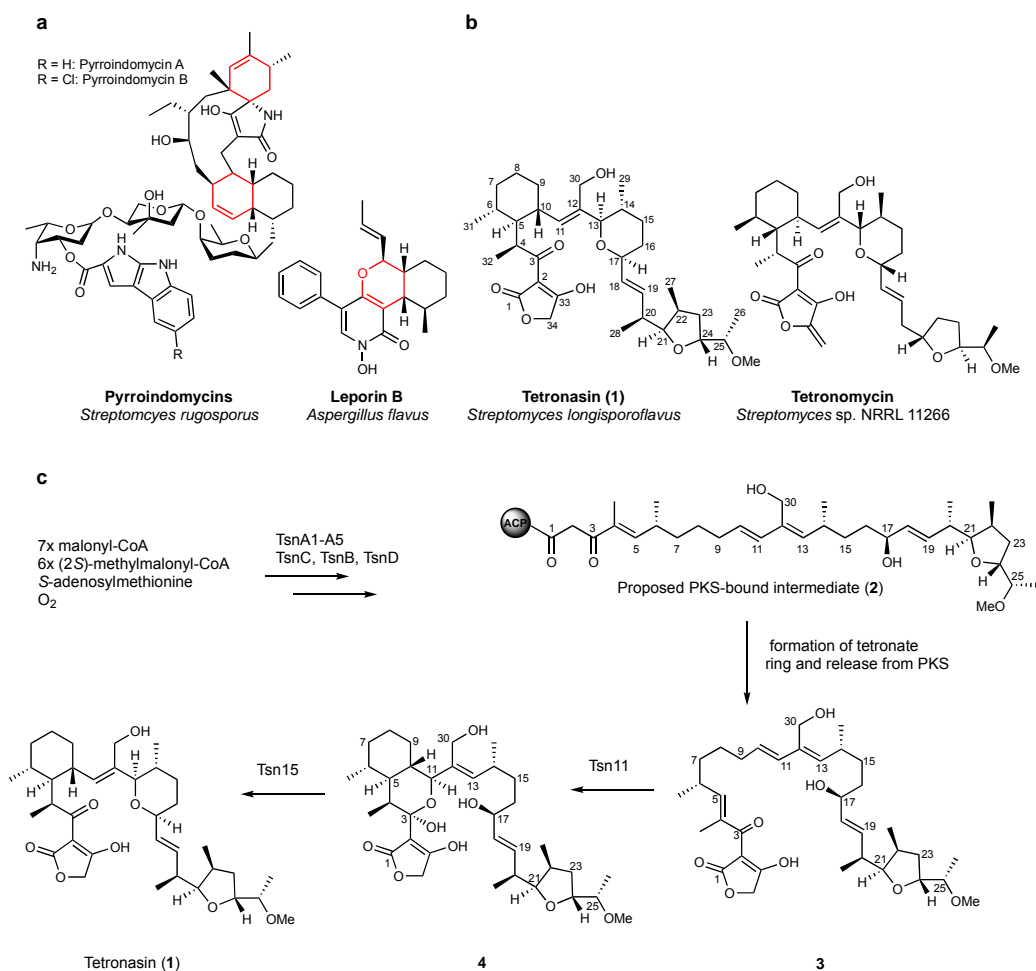
Fig. 1 | [4+2] cyclases in polyether tetronate biosynthesis. a, Structures of pyrroindomycin and leporin B, two polyketide natural products that require a [4+2] cyclase in their biosynthesis to create the rings highlighted in red. **b**, Structures of the polyether tetronate antibiotics tetronasin (**1**) and tetronomycin. **c**, Proposed role of the [4+2] cyclase homologues Tsn11 and Tsn15 in tetronasin biosynthesis.

71 Tetronasin (**1**) (Fig. 1b) from *Streptomyces longisporoflavus*, which has found use as

72 an antibiotic and antiparasitic agent, is an unusual polyether ionophore containing an

73 acyltetronic acid moiety[15]. It bears a near mirror-image structural relationship to

74 tetronomycin (*tmn*) from *Streptomyces* sp. NRRL 11266[16], whose biosynthesis has

75 been shown to involve assembly of the polyketide backbone on a modular polyketide

3

76 synthase (PKS)[16], with release of the chain *via* tetronic acid ring formation[17].

77 Formation of the tetrahydrofuran ring occurs by epoxidation followed by ring-

78 opening and concomitant cyclisation by an epoxide hydrolase[16]. The origins and the

79 timing of central cyclohexane and tetrahydropyran rings remain unknown, although a

80 plausible metal-assisted cascade mechanism has been suggested in which both rings

81 are formed in a single step following release of the polyketide chain from the PKS[18,19].

82

83 Intrigued by the biosynthetic mystery of the origin of the two central rings, herein we

84 show that the cyclohexane and tetrahydropyran rings of tetronasin are formed in a

85 two-step enzymatic cascade reaction. The two enzymes responsible, Tsn11 and Tsn15,

86 are homologues of [4+2] cyclases enzymes found in complex spirotetronate/tetramate

87 pathways. Using a tetronasin precursor isolated from a *S. longisporoflavus* Δtsn11

88 mutant (**3**), we show that Tsn11 catalyses an apparent inverse-electron-demand

89 hetero-Diels-Alder reaction of this species to produce an unexpected oxadecalin

90 intermediate (**4**). Tsn15 then catalyses a rearrangement that forms the tetrahydropyran

91 ring and dismantles the oxadecalin moiety, producing tetronasin. To gain insight into

92 the structure and mechanism of Tsn15, a 1.7 Å crystal structure of a Tsn15-substrate

93 complex was solved. Mutagenesis experiments then indicated that, like its

94 homologues that catalyse [4+2] cycloadditions, Tsn15 also uses a pericyclic

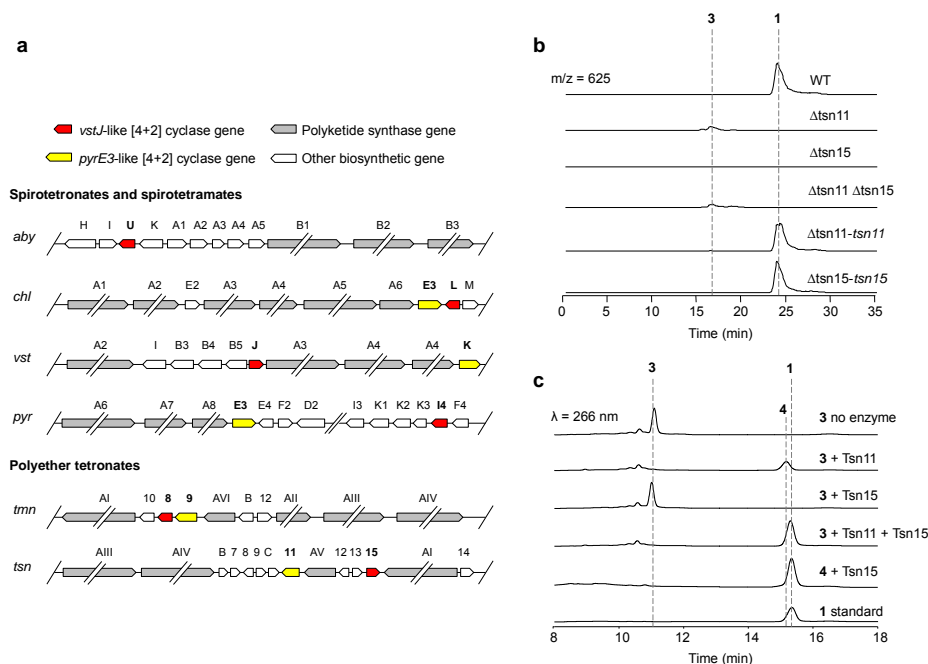95 mechanism for ring formation.

96

97

98

99

100

101 **Results**

102

103 **The PKS-bound linear intermediate of tetronasin.** We have re-analysed the

104 previously sequenced tetronasin biosynthetic gene cluster (GenBank: FJ462704) (*tsn*)

105 (Supplementary Figure 1) and used domain analysis of the PKSs to predict the

106 structure of the hypothetical full-length polyketide (Supplementary Figure 2). To

107 investigate whether further enzymatic reactions tailor the structure before release

108 from the PKS enzymes, we used a chemical probe (methyl 6-decanamido-2-fluoro-3-

109 oxohexanoate **6**[20] designed to intercept PKS-bound intermediates *in vivo* on the *tsn*

110 PKS enzymes. In doing so we detected an incomplete undecaketide polyketide chain

111 in which tetrahydrofuran ring formation, C-25 O-methylation and hydroxylation at C-

112 30 had all apparently occurred, forming **2**, the postulated PKS-bound intermediate

113 (Fig. 1c, Supplementary Figure 3). While we cannot rule out that these enzymatic

114 modifications occurred after being offloaded by **6***,* the detection of **2** strongly suggests

115 that they occur before polyketide chain release from the PKS enzymes, as previously

116 established for other polyethers[21].

117

118 **[4+2] cyclase homologues present in the tetronasin biosynthetic gene cluster.** The

119 tetronasin cluster includes a gene, *tsn11*, which is the homologue of *tmn9* (38%

120 identity at the protein sequence level), previously shown to be essential for

121 tetronomycin biosynthesis[16]. Intriguingly, both of these gene products show

122 significant sequence similarity to the monooxygenase-like [4+2] cyclases that catalyse

123 dialkyldecalin formation in the biosynthetic pathways to the spirotetramate

124 pyrroindomycin (PyrE3)[11] and the spirotetronates versipelostatin (VstK)[9] and

125 chlorothricin (ChlE3)[11] (42-44% protein sequence identity) (Fig. 2a, Supplementary

126 Figure 4). Like PyrE3, Tsn11 contains mutations in several of the four positively

127 charged amino acids (typically arginine) involved in interacting with NADPH[22,23],

128 immediately suggesting that it is not a functional monooxygenase (Supplementary

129 Figure   4).

130

139

140 Co-located with *tsn11* is a second, previously unannotated, gene *tsn15* which also has

141 a counterpart in the *tmn* cluster (*tmn8*)[16]. The products of the latter two genes

142 resemble a second family of Diels-Alderase-like cyclases (VstJ, PyrI4, and AbyU)

143 which create the spiro moiety in spirotetronates and spirotetramates[9–11] (Fig. 2a,

144 Supplementary Figure 5).

145

146   **Tsn11 and Tsn15 are essential for tetronasin biosynthesis.** To analyse the potential

147   roles of Tsn15 and Tsn11 in the biosynthesis of tetronasin (which contains neither a

148   dialkyldecalin nor a spirotetronate moiety), we specifically deleted each gene in *S.*

149   *longisporoflavus* (Supplementary Figure 6). LC-MS analysis of fermentation extracts

150   (Fig. 2b) showed that deletion of either gene abolished tetronasin production, and that

151   complementation *in trans* using the wildtype gene restored production in both cases.

152   In the Δtsn11 mutant a new metabolite, **3**, with the same molecular weight as

153   tetronasin **1** accumulated which was also produced by a Δtsn11 Δtsn15 double mutant

154   (Fig. 2b, Supplementary Figure 6c), implying that Tsn11 acts before Tsn15. The new

155   metabolite was isolated from the Δtsn11 mutant and its structure was determined

156   using mass spectrometry and NMR spectroscopy to be **3** (Fig. 1c, Supplementary

157   Figures 7a, 8, 9, 24-29, Supplementary Table 1, Supplementary Note 1). The new

158   metabolite **3** differs from **1** in lacking both central six-membered rings of tetronasin,

159   directly implicating Tsn11 and Tsn15 in catalysing ring formation as the final steps of

160   the biosynthetic pathway.

161

162   ***In vitro* reconstitution of the cyclohexane and tetrahydropyran rings of**

163   **tetronasin.** To attempt *in vitro* reconstitution of **1** from **3**, Tsn11 and Tsn15 were

164   individually expressed and purified from *Escherichia coli* (Supplementary Figure 10).

165   Tsn11 was found to have flavin adenine dinucleotide (FAD) as a tightly bound

166   cofactor (Supplementary Figure 10b). Incubation of **3** with Tsn11 *in vitro* led to its

167   disappearance within 1 h (Fig. 2c) and HPLC-MS analysis showed the accumulation

168   of a new compound **4**. Tsn11 could not oxidise NADPH or NADH and assaying the

169   activity of Tsn11 pre-incubated with sodium dithionite, to reduce the bound FAD,

170   showed that change in its redox state did not inhibit the reaction of Tsn11 with **3**

171   (Supplementary Figure 11), consistent with previous reports[11,22] that bound FAD is a

172   passive spectator in the active site of flavocyclase PyrE3 in pyrroindomycin

173   biosynthesis. The incubation of **3** with Tsn11 was scaled up to isolate larger amounts

174   of **4**, and its structure was determined by mass spectrometry and NMR spectroscopy

175   analysis (Fig 1c, Supplementary Figures 7b, 12, 13, 30-35, Supplementary Table 2,

176   Supplementary Note 2). Like **3**, compound **4** still lacks the tetrahydropyran ring but

177   the cyclohexane ring has closed within an unexpected oxadecalin hemiacetal moiety.

178   The formation of an oxadecalin intermediate by Tsn11 is strikingly reminiscent of the

179   formation of carbocyclic decalin rings catalyzed by its [4+2] cyclase homologs

180   (PyrE3, ChlE3) in spirotetronate/spirotetramate biosynthesis[11].

181

182   Conversion of **4** into **1** requires dehydration of the hemiacetal, fragmentation of the

183   oxadecalin ring, and a bond to form between the C17-OH and C13 to form the

184   tetrahydropyran ring. Remarkably, incubation of **4** with Tsn15 alone, or of **3** with

185   both Tsn11 and Tsn15, led to complete conversion to **1** within 10 minutes (Fig. 2c,

186   Supplementary Figures 13, 14), Neither the Tsn11- nor the Tsn15-catalyzed reaction

187   proceeded in the absence of enzyme. Despite the evident similarity between the

188   tetronasin and tetronomycin pathways, purified Tmn9 could not substitute for Tsn11

189   in the assay, nor could purified Tmn8 substitute for Tsn15 (Supplementary Figure 16).

190

191   To probe the timing of cyclohexane and tetrahydropyran formation, the Δtsn11 and

192   Δtsn15 mutant strains of *S. longisporoflavus* were treated *in vivo* with the chemical

193   probe **6** [20]. Exactly the same partially-assembled polyketide species were observed as

194   from wildtype cells (Supplementary Figure 3). These data are consistent with the view

195   that tetronate and tetrahydrofuran ring formation, C30-hydroxylation, and C25-O-

8

196   methylation may precede tetrahydropyran and cyclohexane formation. **3** and **4** are

197   therefore likely true biosynthetic intermediates *in vivo* and the central six-membered

198   rings of tetronasin are formed after polyketide chain release, as final steps in the

199   pathway. Between them, these two enzymes establish the configuration at four

200   asymmetric centres in tetronasin[24].

201

202   Cycloadditions of 1-*oxa*-1,3-butadienes *via* inverse-electron-demand hetero-Diels–

203   Alder reactions are important transformations in synthetic chemistry[25,26], so an

204   enzymatic counterpart like Tsn11 is of considerable interest. The formation of *trans*-

205   oxadecalin **4** seems consistent with such a mechanism, but a stepwise process cannot

206   be ruled out (Supplementary Figure 17). Likewise, alternative mechanisms are

207   possible for the reaction catalysed by Tsn15 to convert **4** into **1** (Supplementary

208   Figure 17). A previous isotope feeding study established that the ketone oxygen atom

209   at C3 is derived from propionate rather than water[15], indicating that any mechanism in

210   which the C3 oxygen is derived from water is unlikely (Supplementary Figure 17).

211

212   **The structure of Tsn15.** We propose that Tsn11, like its spirotetronate/spirotetramate

213   homologs, catalyses a [4+2] cycloaddition even though the resulting ring is latent, that

214   is, does not appear in the final antibiotic structure. The structure and mechanism of

215   Tsn11 is currently under investigation. To gain insight into the specificity and

216   mechanism of the unusual transformation catalysed by Tsn15, we have solved the

217   crystal structure of Tsn15 at 1.8 Å using SAD phasing (Fig. 3), and also that of a

218   Tsn15-substrate 1:1 complex, obtained by co-crystallisation of Tsn15 and **4**, at 1.7 Å

219   (Fig. 5).

220

9
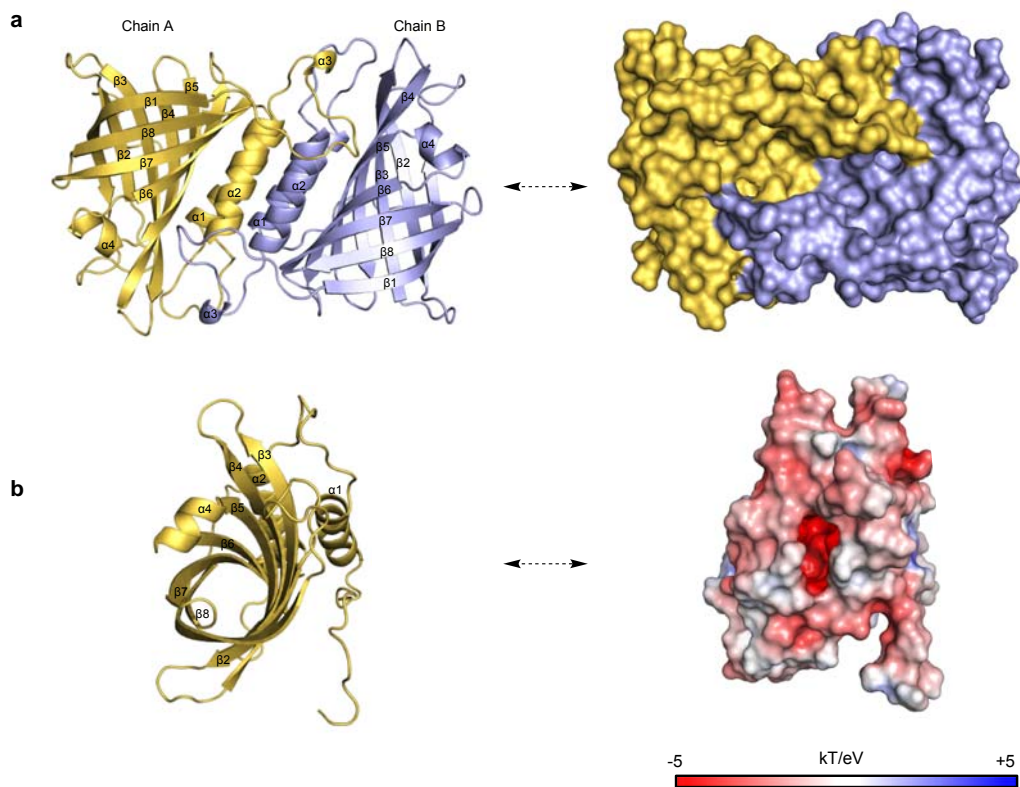
Fig 3 | Crystal structure of Tsn15. The crystal structure of Tsn15 was solved to 1.8 Å resolution using SAD phasing. **a,** Ribbon and surface representation of the homodimeric Tsn15. **b.** The active-site cavity within the β-barrel of Tsn15. Right: surface charge representation contoured at ±5 kT/eV; blue/red.

Consistent with its quaternary structure in solution (Supplementary Figure 18), Tsn15 crystallised as a homodimer of two antiparallel-facing monomers (Fig. 3a). Each monomer chain consists of an *N*-terminal α-helical dimerisation region (α1-α3) followed by an eight-strand β-barrel (β1-β8, α4) enclosing a 388 Å^3 hydrophobic internal cavity (Fig. 3b, Supplementary Figure 19, 20). Each Tsn15 monomer shows the conserved domain fold previously seen in the [4+2] cyclases of spirotetronate and spirotetramate biosynthesis (PyrI4 and AbyU)[10,27], despite low (ca. 20% sequence identity). In addition to these homodimeric [4+2] cyclases, Tsn15 also shares its fold with the homotrimeric allene oxide cyclase enzymes, which catalyse a 4π electrocyclisation (pericyclic) reaction in jasmonic acid biosynthesis[28,29], and PodA,

236   an unusual pyocyanin demethylase from *Mycobacterium fortuitum*[30]. The different

237   activities of these homologous enzymes demonstrate remarkable ability of this protein

238   fold to catalyse a diverse range of reactions (Fig. 4).
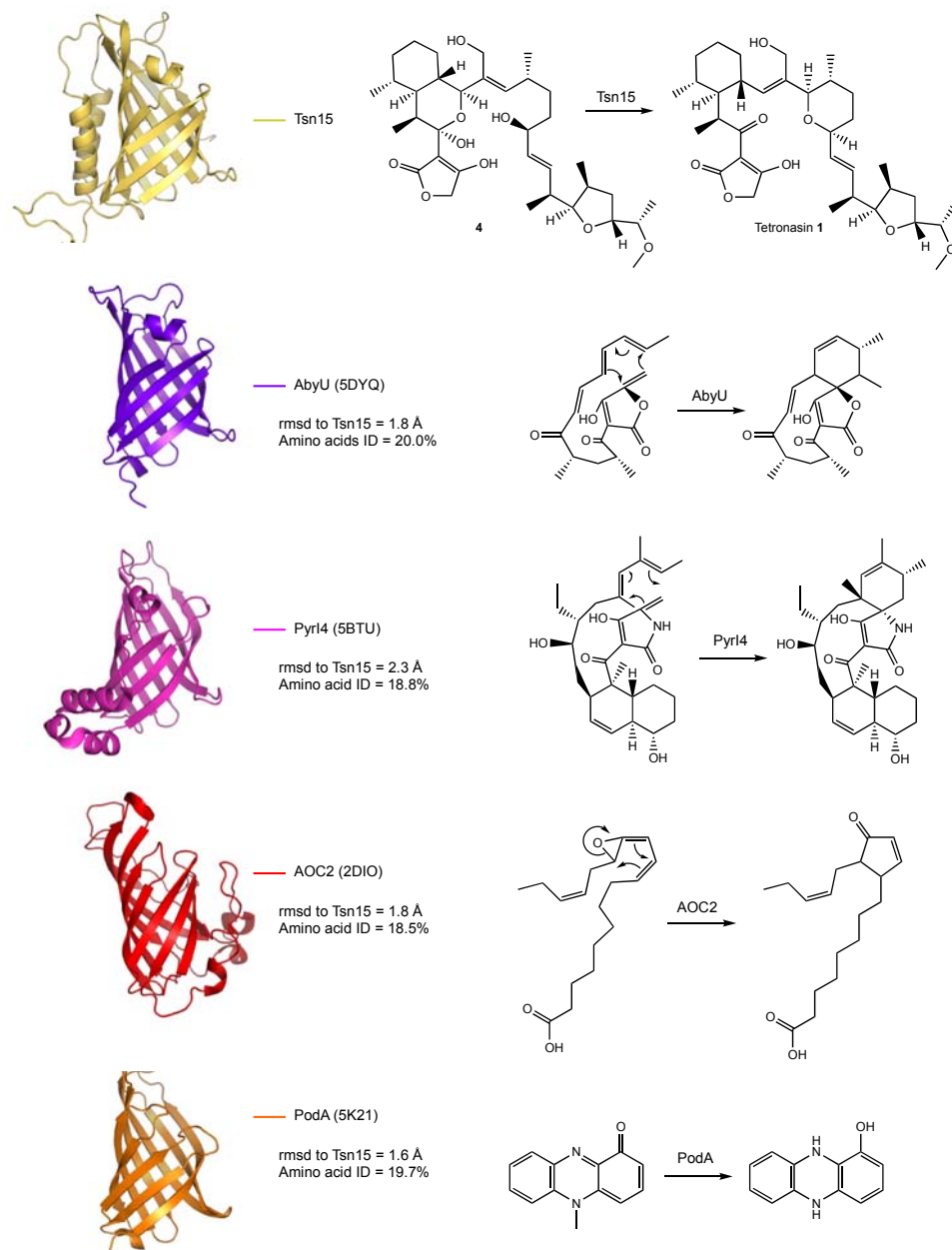
239

240   **Fig. 4 | Structural homologues of Tsn15 and their respective reactions.** The Cα chain of Tsn15 was aligned with its

241   structural homologues AbyU, PyrI4, AOC2, and PodA. Beside each structure is its rmsd value to Tsn15, amino acid identity (%)

242   to Tsn15, and the reaction it catalyses.

243

244   There are no significant conformational differences between the Cα chains of the two

245   crystal structures (Supplementary Figure 21). In the Tsn15-substrate co-crystal the

246   hemiacetal C3 hydroxyl of **4** had undergone dehydration to produce **5** (Fig. 5a). The

247   tetronate ring of **5** is fully inserted into the β-barrel cavity of Tsn15, with the

248   tetrahydrofuran moiety protruding into the solvent (Fig. 5b). The sidechains of amino

249   acid residues S142 and Q164 form hydrogen bonds to the tetronate of **5** (Fig. 5c) and

250   R89 is hydrogen-bonded to the C30-OH (chain B only) (Supplementary Figure 22).

251
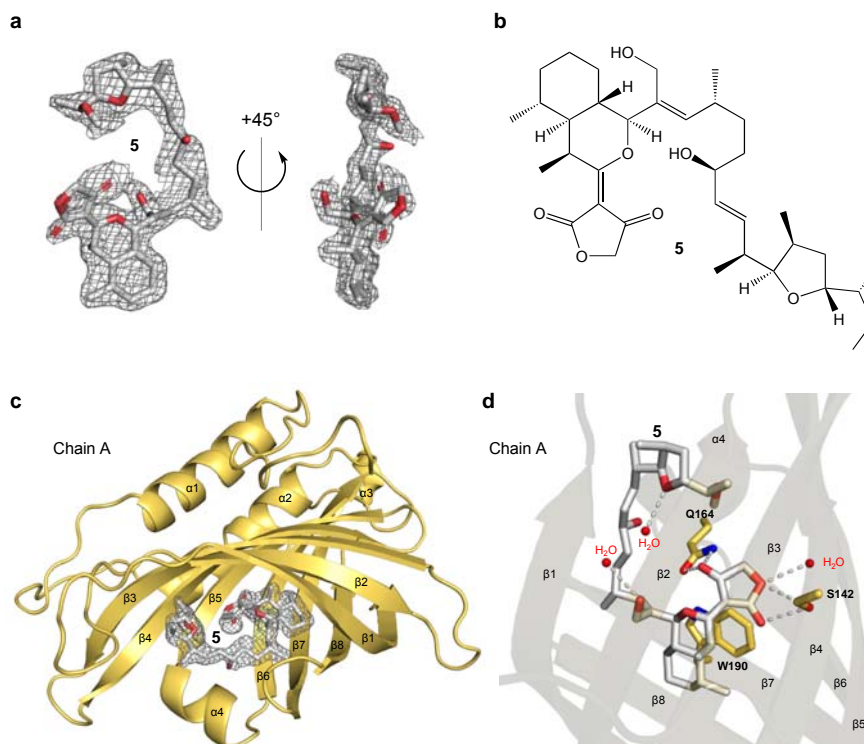
252

253   **Fig. 5 | Structure of Tsn15 and a Tsn15-substrate complex. a,** F_o-F_c of **5** (contoured to 2.0 σ) and its chemical structure.

254   **b,** Tsn15 in complex with intermediate **5**. The F_o-F_c map of **5** could be clearly assigned in the β-barrel cavity of Tsn15 chain A.

255   Contouring to 2.0 σ. **c,** The detailed binding interactions between intermediate **5** and the internal β-barrel residues of Tsn15

256   (chain A) are shown. The dotted grey lines represent hydrogen bonding.

257

258

259 Our initial hypothesis was that Tsn15 might use acid/base catalysis to activate the C-

260 17 hydroxyl and promote nucleophilic ring closure of the tetrahydropyran ring.

261 However, mutagenesis of individual acidic and basic amino acid residues within the

262 β-barrel (R89, E109, and D122) showed that none are essential for Tsn15 activity

263 (Supplementary Figure 23). Further alanine mutagenesis highlighted W190 (essential)

264 and Q164 (mutant shows ca. 30% wildtype activity) both of which are likely

265 important for substrate binding and selectivity (Supplementary Figure 23). W190

266 appears to orient the oxadecalin moiety of **5** through π-stacking interactions (an

267 equivalent tryptophan is conserved in Tmn8, suggesting a conserved role in binding

268 oxadecalin polyether tetronate intermediates) (Fig. 5c, Supplementary Figure 5). The

269 12 *N*-terminal amino acids of Tsn15 do not form an essential substrate-enclosing lid[26],

270 as removing these residues did not abolish enzyme activity as in the case of PyrI4[27]

271 (Supplementary Figure 23). The inability to identify essential general acid/general

272 base catalytic residues suggests that the active site of Tsn15 is primarily a

273 hydrophobic pocket that promotes a reactive conformation, possibly producing the

274 tetrahydropyran ring via a pericyclic rearrangement (Fig. 6) similar to the

275 mechanisms proposed for its homologue AOC2[28] and the [4+2] cyclases PyrI4[27]and

276 AbyU[10]. One complication with this proposal is that the conformation of **5** in the

277 active site appears to be inert for tetrahydropyran formation, with the atoms that must

278 form a bond, C13 and the oxygen of the C17 hydroxyl, being 4.6 Å apart. A possible

279 explanation for this could be that the conformational rigidity imposed on Tsn15 when

280 it crystallised prevented **5** from adopting a near attack conformation. It is also notable

281 that **5** is present in the active site of Tsn15 rather than **4** or tetronasin **1**. We had

282 thought it more likely that **4** would be converted by Tsn15 and tetronasin **1** would

283 therefore cocrystallise in its active site, analogous to the PyrI4 cocrystallisation

13

284　experiments[27]. One explanation for this could be that **5** is an inert spontaneous

285　dehydration product of **4,** the true substrate. If **4** is the true substrate, however, then

286　tetrahydropyran formation and dehydration at C3 must occur simultaneously

287　(Supplementary Figure 17b), which would likely require an acidic residue to donate a

288　proton to the hemiacetal hydroxyl, thereby creating a better leaving group. However,

289　as demonstrated, the acidic groups in the active site are not essential and no acidic

290　amino acid is adjacent to C3, so it is not clear how this could occur. While we cannot

291　rule out **5** being inert, in our view **5** is more likely to be the Tsn15 substrate as the

292　dehydration of **4** to form **5** should be a favourable first step for tetronasin formation.

293　Dehydration of the hemiacetal hydroxyl (whether spontaneous or Tsn15 catalysed)

294　would stabilise the anion that forms at the C3 oxygen during tetrahydropyran

295　formation through conjugation with the C1 and C33 carbonyl groups (Supplementary

296　Figure 17a, 17c, 17e). While the exact mechanism used by Tsn15 to convert **4** into

297　tetronasin remains unknown, our data is more consistent with Tsn15 catalysing a

298　pericyclic rearrangement rather than a nucleophilic acid/base reaction (Fig. 6).

299　Regardless, the crystal structure of Tsn15 with **5** in its active site delineates the

300　substrate-binding residues of Tsn15 and provides a robust foundation for conducting

301　future mechanistic studies on this fascinating class of cyclase.

302

303

304

305
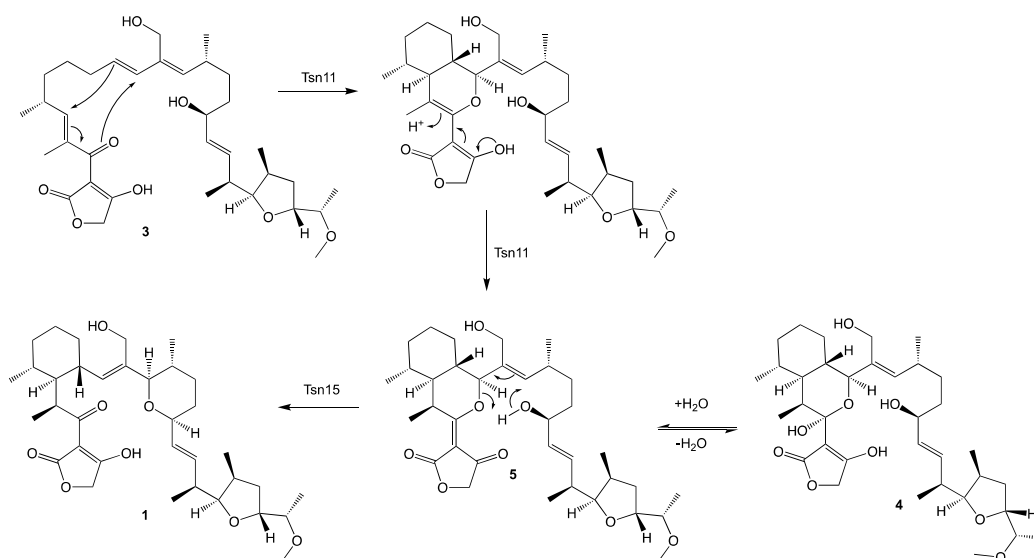
306

Fig. 6 | Proposed mechanism for formation of the cyclohexane and tetrahydropyran rings of tetronasin. Tsn11 catalyses an inverse-electron-demand hetero-Diels-Alder reaction to form an oxadecalin intermediate. The oxadecalin is hydrated to form the cyclic hemiacetal **4** which was purified from the Tsn11 + **3** assay and structurally characterised. Tsn15 then catalyses dehydration of **4** to form **5** (which crystallised in the active site of Tsn15), followed by a pericyclic rearrangement to form the tetrahydropyran ring and fragment the oxadecalin, producing tetronasin **1**.

312

Our results show that the standalone enzyme Tsn11 catalyses a previously unsuspected intramolecular [4+2] cycloaddition that, in formal terms, represents an inverse-electron-demand hetero-Diels-Alder reaction[26] and which constitutes a latent but compelling mechanistic link with spirotetronate and spirotetramate biosynthesis. Likewise, Tsn15, structurally homologous to known Diels-Alderase-like cyclases, has evolved to catalyze a different, but possibly also a pericyclic, transformation. From a synthetic biology perspective, these enzymes could be useful for stereospecifically synthesising cyclohexane and tetrahydropyran moieties in synthetic polyether ionophore analogues. The tolerance of Tsn15 to mutations in its active site and the diverse range of reactions catalysed by its protein fold (Fig. 4) further suggests it may have some potential as a biotransformation catalyst. Meanwhile, these findings

324   suggest that further examples of novel, and potentially latent, enzymatic pericyclic

325   reactions remain to be discovered in natural product biosynthetic pathways.

326
327
328
329
330
331
332
333
334
335
336
337
338
339
340
341
342
343
344
345
346
347
348
349
350
351
352
353
354
355
356
357
358
359
360
361
362
363
364
365
366
367
368
369
370
371

372   **Methods**

373

374   <u>Material, bacterial strains and culture conditions</u>

375

376   All chemicals and biomaterials were purchased from Merck (USA) or Thermo Fisher

377   (USA) unless otherwise stated. All the enzymes were purchased from Thermo Fisher

378   (USA) or New England Biolabs (USA). All *E. coli* strains were grown in liquid or on

379   solid (1.5% agar) LB medium at 37 °C. For general maintenance of strain stocks, *S.*

380   *longisporoflavus* was grown in grown at 30 °C 220 rpm in TSBY (30 g/L tryptic soy

381   broth, 5 g/L yeast extract, 103 g/L sucrose) or at 30 °C on SFM agar (20 g/L soy flour,

382   20 g/L D-mannitol, 20 g/L agar).

383

384   <u>General DNA manipulation techniques</u>

385

386   PCR amplification of DNA was performed using Q5 DNA polymerase (New England

387   Biolabs). DNA cloning was performed using standard restriction digestion or

388   isothermal DNA assembly. Sanger sequencing was used to confirm the sequence of

389   all cloned DNA. Genomic DNA from *S. longisporoflavus* was isolated by chloroform

390   extraction followed by isopropanol precipitation and washed using 70% ethanol.

391   Mutagenesis of *tsn15* was performed for *tsn15*-E109A, *tsn15*-D122A, and *tsn15*-

392   W190A using a Quikchange II mutagenesis kit (Agilent, USA). The remaining *tsn15*

393   mutant constructs were ordered from GenScript (China).

394

395

396   <u>Deletion and complementation of *tsn11* and *tsn15* in *S. longisporoflavus*</u>

397

398   The deletions of *tsn11* and *tsn15* were made in the coding region to avoid introducing

399   a frameshift that could have deleterious polar effects on downstream gene expression.

400   Genomic DNA of *S. longisporoflavus* was purified and used as a template for all PCR

401   amplification necessary to create a *tsn11* gene-deletion plasmid construct. 2 kbp

402   stretches of the genomic DNA upstream and downstream of *tsn11* were amplified

403   using tsn11_Up_Fw/tsn11_Up_Rv and tsn11_Dn_Fw/tsn11_Dn_Rv primers,

404   respectively. The primers contained additional nucleotides on their 5' ends that

405   enabled the two fragments to be joined and ligated into the *Nde*I site of pYH7 using

406   isothermal DNA assembly[43], producing the recombinant construct pYH7-*tsn11* in

407   which 1356 nt of the *tsn11* coding frame was deleted. pYH7-*tsn11* was transformed

408   into *E. coli* ET12657/pUZ8002[44] cells which were mixed into a fresh liquid culture of

409   *S. longisporoflavus*. After mixing, the cell mixture was plated on SFM agar

410   supplemented with 20 mM $MgCl_2$ and incubated at 30 °C for 16 h. The SFM agar was

411   then overlayed with 1 mL of sterilised water containing nalidixic acid and apramycin

412   (0.875 mg of each per 35 mL plate). After several days of growth at 30 °C,

413   apramycin-resistant *S. longisporoflavus* exconjugants containing a single homologous

414   crossover event with pYH7-*tsn11* appeared. These single colonies were grown of

415   SFM agar lacking antibiotics to promote a second recombination event via plasmid

416   loss. *S. longisporoflavus* exconjugants that had undergone a double homologous

417   crossover event (those that had regained apramycin sensitivity) were screened using

418   tsn11_KO_Fw/tsn11_KO_Rv primers to detect the 572 bp PCR product indicative of

419   the successful genomic deletion of *tsn11*. The PCR product was sequenced to confirm

420   the *S. longisporoflavus* Δtsn11 genotype.

421

422   For the deletion of Tsn15, genomic DNA of *S. longisporoflavus* was purified and used

423   as a template for all PCR amplification necessary to create a *tsn15* gene-deletion

424   plasmid construct. 2 kbp stretches of the genomic DNA upstream and downstream of

425   *tsn15* were amplified using tsn15_Up_Fw/tsn15_Up_Rv and

426   tsn15_Dn_Fw/tsn15_Dn_Rv primers, respectively. The primers contained additional

427   nucleotides on their 5' ends that enabled the two fragments to be joined and ligated

428   into the *Nde*I site of pYH7 by Gibson assembly[43], producing the recombinant

429   construct pYH7-*tsn15* in which the entire 621 bp *tsn15* coding frame was deleted. The

430   protocol for deleting *tsn15* was then identical to that previously described for

431   creationg *S. longisporoflavus* Δtsn11. Exconjugants that had undergone two

432   homologous crossing over events with pYH7-*tsn15* were screened using

433   tsn15_KO_Fw/tsn15_KO_Rv primers to detect the 713 bp PCR product indicative of

434   the successful genomic deletion of *tsn15*. The PCR product was sequenced to confirm

435   the *S. longisporoflavus* Δtsn15 genotype.

436

437   The *S. longisporoflavus* Δtsn11 Δtsn15 (double mutant) was created by deleting *tsn15*

438   in *S. longisporoflavus* Δtsn11. The same protocol for deleting *tsn15* was followed,

439   except that *S. longisporoflavus* Δtsn11 rather than wildtype *S. longisporoflavus* 83E6

440   was conjugated with pYH7-*tsn15*.

441

442   To complement the *S. longisporoflavus* Δtsn11 mutant, *tsn11* was amplified from the

443   genomic DNA of *S. longisporoflavus* using tsn11-pIB139-Fw/tsn11-pIB139-Rv

444   primers. The amplified *tsn11* was then cloned by isothermal DNA assembly at the

445   *Xba*I site of pIB139, downstream of the *ermE*[*] promoter, creating pIB139-tsn11.

446   pIB139-tsn11 was conjugated into *S. longisporoflavus* Δtsn11 using *E. coli*

447   ET12657/pUZ8002. Apramycin-resistant exconjugants were selected and grown for

448   seven days before HPLC-MS analysis. To complement the *S. longisporoflavus* Δtsn15

449   mutant, *tsn15* was amplified from the genomic DNA of *S. longisporoflavus* using

450   tsn15-pIB139-Fw/tsn15-pIB139-Rv primers. The amplified *tsn15* was then cloned by

451   isothermal DNA assembly at the *Xba*I site of pIB139, downstream of the *ermE*[*]

452   promoter, creating pIB139-tsn15. pIB139-tsn15 was conjugated into *S.*

453   *longisporoflavus* Δtsn15 using *E. coli* ET12657/pUZ8002.

454

455   <u>Analysis of metabolites from *S. longisporoflavus*</u>

456

457   To test for the production of either tetronasin **1** or intermediate **3**, a colony of *S.*

458   *longisporoflavus* (or of a *S. longisporoflavus* deletion mutant/complementation strain)

459   was inoculated into tsn-medium-A (30 g/L tryptic soy broth, 3 g/L $CaCO_3$, trace

460   elements: 4 mg/L $FeSO_4$, 4 mg/L $ZnSO_4$, 0.6 mg/L $CuSO_4$, 0.4 mg/L $MnSO_4$, 0.4

461   mg/L $KMoO_4$) and grown for two days at 30 °C 200 rpm. The culture was then plated

462   onto petri dishes containing tsn-medium-B (30 g/L tryptic soy broth, 3 g/L $CaCO_3$,

463   100 g/L dextrin, 20 g/L agar, trace elements: 4 mg/L $FeSO_4$, 4 mg/L $ZnSO_4$, 0.6 mg/L

464    $CuSO_4$, 0.4 mg/L $MnSO_4$, 0.4 mg/L $KMoO_4$) and grown at 30 °C for seven days. The

465   agar and cells were then extracted using ethyl acetate. The ethyl acetate was

466   evaporated under reduced pressure and the organic extract was dissolved in methanol

467   for analysis HPLC (Hewlett Packard, Agilent Technologies1200 series) coupled to a

468   mass spectrometer (Thermo Finnigan MAT LTQ). The HPLC-MS was fitted with a

469   250 mm x 4.6 mm 5μm C18 reverse-phase column (5μ OSD3, 100Å. Phenomenex,

470   USA). The mobile phase comprised of 20 mM ammonium acetate and increasing

471   methanol at a flow rate of 0.7 mL/min: 0-5 min, 5-75% methanol; 5-30 min, 75-95%

472 methanol, 30-34 min, 95% methanol 35-36 min, 95-5% methanol. Normalised

473 collision energy of 35% was used for the molecular fragmentation of tetronasin. High-

474 resolution mass spectra were obtained using a Vion IMS QTOF (Waters, USA)

475 operated by the mass spectrometry service of the Department of Chemistry,

476 University of Cambridge.

477

478 <u>Heterologous expression of cyclase genes in *E. coli*</u>

479

480 The *tsn15*, *tsn11*, *tmn9*, and *tmn8* genes were each amplified by PCR. The PCR

481 products were individually digested using *Nde*I and *Xho*I and cloned between the

482 *Nde*I and *Xho*I sites of pET28a(+), in-frame with the *N*-terminal polyhistidine tag

483 (MGSSHHHHHHSSGLVPRGSH). Each expression plasmid was individually used to

484 transform chemically competent *E. coli* BL21 (DE3) cells (Thermo Fisher, USA). A

485 single colony from each *E. coli* BL21 (DE3) transformant was cultured at 37 °C, 200

486 rpm in lysogeny-broth (LB) containing 50 µg/mL kanamycin. Once the culture had

487 reached an A_{600} = 0.5, protein expression was induced by adding isopropyl β-D-1-

488 thiogalactopyranoside (IPTG) to a final concentration of 0.5 mM. The culture was

489 then incubated for 16 h at 20 °C, 200 rpm. The cells were harvested by centrifugation

490 and resuspended in 30 mL of 20 mM Tris-Cl pH 7.9 buffer, 500 mM NaCl). Cells

491 were lysed using an Emulsiflex C5 (Avestin, Canada) according to the manufacturer's

492 instructions. The insoluble fraction was removed by centrifugation and the soluble

493 fraction was passed though Ni-affinity resin (Qiagen, Germany) to bind the

494 recombinant protein. Lysis buffer containing increasing imidazole concentrations (50-

495 400 mM) was used to remove contaminants and subsequently elute pure recombinant

496 protein (monitored by SDS-PAGE). Fractions containing the purified recombinant

497   proteins were concentrated using Amicon Ultra-15 centrifugal filter units (Merck

498   Millipore, USA) and the buffer was exchanged into 20 mM Tris-Cl, 100 mM NaCl,

499   10% glycerol pH 7.9 using a PD-10 column (GE Healthcare, USA) according to the

500   manufacturer's instructions. Protein concentration was determined by the Bradford

501   assay using a BSA standard curve. Protein aliquots were then snap frozen in liquid

502   nitrogen and stored at -80°C.

503

504   <u>Protein quaternary structure analysis by analytical ultracentrifugation</u>

505

506   Analytical ultracentrifugation (AUC) was used to measure the molecular weight of

507   Tsn11 and Tsn15 in solution. Tsn15 and Tsn11 were purified and individually

508   concentrated to 0.75 mg/mL in a final volume of 800 µL. When Tsn11 and Tsn15

509   were sedimented together, each was present in the same chamber at a concentration of

510   0.75 mg/mL. AUC experiments were performed using an Optima XL-I (Beckman

511   Coulter, USA) centrifuge fitted with an An60 Ti four-hole rotor. Absorbance and

512   interference data were acquired in the continuous mode at time intervals of 170 s and

513   at a rotor speed of 40,000 rpm, at 20 °C with systematic noise subtracted, but without

514   averaging. The density and viscosity of the buffer (20 mM Tris-Cl pH 7.9, 100

515   mM/150 mM NaCl) and the partial specific volume of the protein were both

516   calculated using Sednterp[32]. The multi-component sedimentation coefficient

517   distributions were obtained from 128 scans by direct boundary modeling of the Lamm

518   equation using Sedfit v.14.1.

519

520

521

<u>Isolation of Intermediate **3** for NMR analysis</u>

523

524   Intermediate **3** was isolated from *S. longisporoflavus* Δtsn11. Well-grown *S.*

525   *longisporoflavus* Δtsn11 colonies were inoculated into 5 mL of tsn-medium-A and

526   grown for two days at 30 °C and 200 rpm. The cultures were then inoculated into

527   flasks containing 50 mL of tsn-medium-A and grown for an additional two days at

528   30 °C 200 rpm, or until a thick mycelial culture had grown. These cells were plated

529   on 400 12 cm x 12 cm agar plates each containing 50 mL of tsn-medium-B agar (30

530   g/L tryptic soy broth, 3 g/L $CaCO_3$, 100 g/L dextrin, 20 g/L agar, trace elements: 4

531   mg/L $FeSO_4$, 4 mg/L $ZnSO_4$, 0.6 mg/L $CuSO_4$, 0.4 mg/L $MnSO_4$, 0.4 mg/L $KMoO_4$)

532   and grown for seven days at 30 °C. The agar was then cut into small squares and

533   combined in a large glass flask where it was extracted three times by submerging in 2

534   L of ethyl acetate . The ethyl acetate was evaporated under reduced pressure to yield 7

535   g of a brown crude organic extract. The crude extract was dissolved in 8 mL of

536   methanol and loaded onto 8 10g/70 mL C18 reverse-phase Isolute cartridges (Biotage,

537   Sweden) according to the manufacturer's instructions. Fractions were eluted from the

538   columns using a mixture of 20 mM ammonium acetate and increasing methanol.

539   Fractions containing intermediate **3** were identified by HPLC-MS and pooled together

540   (1.15 g in total) before a second round of SPE purification. The final purification step

541   was performed using an Infinity II semipreparative HPLC (Agilent, USA) fitted with

542   a Phenomenex (USA) C18 Prodigy column (5 µm ODS-3 100Å, 250 x 10 mm).

543   Gradient elution of intermediate **3** was achieved using a mobile phase of 5 mM

544   ammonium acetate and methanol with a flow rate of 3 mL/min: 0-5 min, 5-75%

545   methanol; 5-15 min, 75-85% methanol; 15-19 min, 85-100% methanol; 19-20 min,

546   100-5% methanol. Fractions containing intermediate **3** were identified by detecting its

547   characteristic chromophore (λ_{max} = 236) nm and pooled together, followed by solvent

548   evaporation under reduced pressure. The dried extract was dissolved in ethyl acetate

549   to remove the ammonium acetate, followed by freeze-drying to yield purified **3** (12.5

550   mg). For structural determination, **3** was dissolved in deuterated chloroform and

551   analysed using a 500 MHz DCH Cryoprobe Spectrometer (Bruker, USA).

552

553

554   <u>Isolation of Intermediate **4** for NMR analysis</u>

555

556   Intermediate **4** was isolated from an *in vitro* reaction of **3** and Tsn11. The assay

557   mixture (60 mL in total) contained: 20 mM Tris-Cl, 100 mM NaCl, pH 7.9 containing

558   50 µM Tsn11, 400 µM of **3**, and 5% v/v methanol. After incubation at 30 °C for 1.5 h,

559   the reaction mixture was extracted six times with 30 mL of ethyl acetate. The ethyl

560   acetate was evaporated, and the organic residue was dissolved in methanol. The

561   extract was chromatographed on semipreparative HPLC as described above. Fractions

562   containing intermediate **4** were identified by detecting its characteristic chromophore

563   (λ_{max} = 254) nm and pooled together for solvent evaporation. The dried residue was

564   dissolved in ethyl acetate to remove the ammonium acetate, followed by freeze-

565   drying to yield purified **4** (3.3 mg). For structural determination, **4** was dissolved in

566   deuterated methanol and analysed using a 500 MHz DCH NMR Cryoprobe

567   Spectrometer (Bruker, USA).

568

569   *In vitro* assays

570

24

571   *In vitro* activity assays of Tsn11 and Tsn15 were performed in 20 mM Tris-Cl buffer,

572   100 mM NaCl, 5% v/v methanol pH 7.9. Typically, reaction volumes were 100 µL

573   and contained 200 µM of **3** or **4**. Tsn11 and/or Tsn15 were added to a final

574   concentration of 5 µM. The reactions were carried out at 30 °C for 1 h unless stated

575   otherwise. The reactions were terminated by adding 400 µL of methanol before being

576   completely dried under reduced pressure. The dried extract was redissolved in 100 µL

577   methanol and analysed by HPLC fitted with a Phenomenex C18 Prodigy column (5

578   µm ODS-3 100Å, 250 x 10 mm) using a gradient program of 20 mM ammonium

579   acetate and increasing methanol at a flow rate of 3 mL/min: 0-5 min, 5-75%

580   methanol; 5-15 min, 75-85% methanol; 15-19 min, 85-100% methanol; 19-20 min,

581   100-5% methanol. For all *in vitro* assays, the identity of intermediates **3** and **4** were

582   confirmed by their unique UV chromophores and MS^3 fragmentation patterns. For

583   analysis of the Tsn11 sodium dithionite assays and the Tsn15 point mutation assays, a

584   Poroshell 120, EC-C18, 27 µM, 46 x 100 mm (Agilent, USA) column eluted with 5

585   mM ammonium acetate and methanol at 1 mL/min: 0-5 min, 5-75% methanol; 5-15

586   min 75-95% methanol; 15-19 min, 95% methanol; 19-20 min, 95-5% methanol.

587   When the Tsn11 activity assay was conducted in the presence of sodium dithionite,

588   100 µM of **3** was used with 1 µM of Tsn11 and 1 mM of sodium dithionite. Parallel

589   reactions were carried out and terminated at 0 min, 2 min, 4 min, and 8 min,

590   respectively.

591

592   <u>Protein crystallisation</u>

593

594   For protein crystallisation, *tsn15* was expressed in *E. coli* BL21 (λDE3) and purified

595   by nickel-affinity chromatography as previously described. The proteins were further

596   purified using a preparative gel-filtration ÄKTA (GE Healthcare Lifescience, USA)

597   connected to a Hiload 16/60 column packed with Superdex 200 resin. Fractions

598   containing Tsn15 were pooled and concentrated. Tsn15 was concentrated to 15

599   mg/mL (20 mM Tris-Cl pH 7.9 buffer, 100 mM NaCl) and crystallised in 0.1 M

600   PCTP (0.1 M each sodium proprionate, sodium cacodylate trihydrate, and bis-Tris

601   propane) pH 6.0, 25% PEG 1500 using the sitting-drop, vapour-diffusion method at

602   19 ºC. The Tsn15-substrate complex was crystallised using hanging-drop, vapor-

603   diffusion method at 18 ºC. To obtain the protein complex, a solution composed of

604   Tsn15 protein (15 mg/mL in 20 mM Tris-Cl pH 7.9 buffer, 0.5 M NaCl) and 10 mM

605   of **4** was incubated for 10 minutes and then crystallised in 0.1 M PCTP pH 6.0 buffer,

606   27% PEG 1500. To solve the phases for the Tsn15 structure, a selenomethionine

607   labeled version of Tsn15 (SeMet-Tsn15) was created and the structure was

608   determined using the Single Anomalous Dispersion (SAD) method. To achieve this, *E.*

609   *coli* BL21 (λDE3) cells transformed with pET28a(+)-*tsn15* were cultured in M9

610   medium. Once the culture had reached A_{600} = 0.5, 0.1 g/L L-lysine, 0.1 g/L L-

611   threonine, 0.1 g/L L-phenylalanine, 0.05 g/L L-leucine, 0.05 g/L L-isoleucine, 0.05

612   g/L L-valine were added to the growing culture, followed by 0.06 g/L of L-

613   selenomethionine. SeMet-Tsn15 was purified and exchanged into buffer containing

614   20 mM Tris-Cl pH 7.9, 100 mM NaCl, 2 mM EDTA, and 2 mM tris(2-

615   carboxyethyl)phosphine (TCEP), then crystallised as before. Crystals were harvested

616   from the crystallisation drop and transferred into a cryoprotecting solution containing

617   the crystallisation solution and 25-27% ethylene glycol. The crystals were then flash-

618   frozen in liquid nitrogen using nylon loops. X-ray diffraction data for SeMet-Tsn15

619   were collected at the Diamond Light Source (DLS) I04 beamline, Oxford, UK, while

620   for the complex Tsn15-substrate data were collected at PETRAIII, beamline 13,

621   Hamburg, Germany. The X-ray data processing was performed using XDS[33] and

622   scaled using Aimless[34] from CCP4 suite[35]. The phases for SeMet-Tsn15 was solved

623   using AutoSol[36] from Phenix suite[37]. The structural model was initially built by

624   AutoBuild[38] also from PHENIX suite[37]. The phases for the Tsn15-substrate complex

625   was determined by molecular replacement using the program Phaser[39] from Phenix

626   suite[37]. The SeMet-Tsn15 structure was used as the search model for molecular

627   replacement. Both SeMet-Tsn15 and Tsn15-substrate complex models were refined

628   using Phenix.refine[40] and further visual inspection and real space refinement was

629   performed by COOT[41]. The stereochemical quality of the models was assessed using

630   MolProbity[42]. The protein structure figures were prepared using PyMOL Molecular

631   Graphics System, Version 2.0 Schrödinger, LLC.

632

633   Revised sequence of Tsn11

634

635   Closer examination of the *tsn11* gene compared to the deposited sequence revealed

636   the start codon to be an additional 12 bp 5' of the previously annotated start codon.

637   The new start codon was a methionine (ATG) rather than a leucine (TTG) and was six

638   bp downstream from a likely Shino-Delgarno sequence (GGAAGAA). The revised

639   protein sequence of the updated Tsn11 is presented below.

640

641

642

643

644

645

646   Tsn11:

647   MEIPLTGTVVIAGAGPVGLFLASELRLAGVEAVVLERSPKANEHTVGGTLHARTADL
648   FDQRGIMDTLRAGNPPLWPRLHFASYWLDLAPHMEDEYSLLLPQQYTEEMLEAHATE
649   LGADIRRGHTCVSLTQDADGVTVGVRADSGDYELRGAYLVGCDGGDSTVRELAAFPV
650   QESGPRWYGLLADVESIEGDWHPGNYPGGQFAVIRSPHEGGPSRIMTLEFNETTQPP
651   PADQPVSVEEVIASTERITGRTPVVGEVQWLHRYTNTTREAENYRQGRVFVAGDAAH
652   LHVAFAGHGLSTGLHDAANLGWKLAAVLDGRAPDSLLDTYDEERRPVGHRACVFTQS
653   QMALLTQGGQQLDILRQLFTDLVKLPEVNHHLITTVTDVRYALDGAEKEDTHPLLGRP
654   VPNQLVKDADGQATAVAEALRAGRGVLIDLTDGAAALPDTSGRRGHLDSVSRGPADA
655   VDATALLVRPDGFVAWAATADTGNDGLEPALRRWFGDTA
656

657   Revised Sequence of Tmn9

658

659   During cloning of *tmn9* it was noted that the sequence differed from that previously

660   published[15] (confirmed by sequencing independent PCR reactions). The revised Tmn9

661   protein sequence is as follows:

662

663   Tmn9:

664   MSEPVVVVGAGPAGLMLACELAMRDVPAVLVDIHPTQRAEAPAMAINAGTLEMLDQR
665   GLAAGLREGTVTFPEVRFADLRLAFEKVQGPREPTHMVLQSRLEKVLIDRAVELGVD
666   LRWATRLTGFEEAADGSGVTVTLASDAGEEQLRCRYLVGCDGRESIVRKQAGIDYVG
667   DDWVIVRGIVGDVAINREDVAPEQYGLSYTDNGDQFLGAPLSPDVMRVFSAEFSTEP
668   PEFEDGPATLEQLGDAVKRLTGKELKATEAHWLQHYSIVTRNAEQYRKGRVFIAGDA
669   AHVHYPYNGQGLGTAIGDAVNLGWKIAAEVHGWAPADLLDSYHVERHLAGRLACMNI
670   QAQLALLYPRPLARYMREMMGEFLKFDEVNVFLAEIVTNLGPAVPIAYEGVPEPVEG
671   DRLLGRRLPKVQIKTADGDMGVAETLQSGRGVLLDLSGDASAQEESGWADRVDVVRA
672   QPVPDLPGTLLLRPDGCVAWHDGGGWGQDELRTALRTWFGAPTG
673

674   Sequence of Tsn15

675   Prior to the submission of this manuscript a different ORF in the tetronasin gene

676   cluster, an ABC transporter, was named Tsn15. The Tsn15 described in this paper

677   was not annotated. As such, the ABC transporter has been renamed Tsn15b and

678   Tsn15 now refers to the [4+2] cyclase homologue. For clarity the DNA and protein

679   sequence of Tsn15 are presented below:

680

681   *tsn15*:

```
682    ATGACCACTTCCATCGATCCGACGACCCCGCTGACCTACAACCCCGTCATCGACGCG
683    CTCGTCGGCTCGTGGCGCCAGATCATCGACGCCGACTACTCGGCGGACGACACCCGG
684    CTGCCCGATCTCGCCGTGCTGGCCCGCTCCACCGCGCGGGCGGTCGCGGCTGCCGTA
685    CCCCGTCCGCTCGCGGAGATCTCGGCCCCGGACGCGCCGGACGAGCGCGGCGAACTC
686    GTGCTGCTGGAGAAGGTGATCCAGGAAGTGGCCGACCGCGAGTACACCCCGCTGAGC
687    CCCGAGGGGCCGAGCGTCGGGGACCTCGTCCTGGTGACGGAGAAGATCTACAACTCC
688    GACCGCGAGGAGATCGGCGCGGACACCGGGCGGCTGCGGATCATCCGCAAGGACCCG
689    GAGACCGGGCACCACTTCACGGTCTCGCTCGTCACGTCCACGGTGCAGGGCAACAAG
690    CTGTTCGCCTTCGGCTACACCGAGATGGAGGCCCAGCTCGCCGGGGGCCGCACCACC
691    ATCCAGGTCGCCTGCTGGGACGGCCCCTGGGCCGGCATGAGCGGCACCCTGTCCTGG
692    GTCATCAACTCCATGACGGCCGCCGAGTCGCGGTACGAGCTGCGCCGCTGA
693

694    Tsn15:

695    MTTSIDPTTPLTYNPVIDALVGSWRQIIDADYSADDTRLPDLAVLARSTARAVAAV
696    PRPLAEISAPDAPDERGELVLLEKVIQEVADREYTPLSPEGPSVGDLVLVTEKIYNS
697    DREEIGADTGRLRIIRKDPETGHHFTVSLVTSTVQGNKLFAFGYTEMEAQLAGGRTT
698    IQVACWDGPWAGMSGTLSWVINSMTAAESRYELRR
699
```

<u>Interception and detection of PKS-bound polyketide intermediates</u>

All *S. longisporoflavus* strains were grown in 10 mL tsn-medium A for 2 days at 30 °C at 200 rpm. Seed cultures (100 μl) were used to inoculate tsn-medium A (10 mL of liquid culture, in duplicate, in 50 mL Erlenmeyer flasks with springs). They were then incubated at 30 °C for 5 days. After the first day of incubation, the probe (methyl 6-decanamido-2-fluoro-3-oxohexanoate (**6**), final concentration: 1 mM) was dissolved in 80 μl of MeOH and added portionwise over 4 days (20 μl each day, days 2-5). Control liquid cultures omitting methyl 6-decanamido-2-fluoro-3-oxohexanoate were also prepared (in duplicate copy). After 5 days of fermentation, the liquid cultures were extracted with ethyl acetate (20 mL). The extracts were concentrated and the residues were redissolved in HPLC-grade methanol (1 mL) for mass spectrometry analysis.

HPLC-HR-ESI-MS analyses of *S. longisporoflavus* extracts were carried out on an LTQ-T Orbitrap Fusion instrument. Reverse phase chromatography was used to

716   separate the mixtures prior to MS analysis. Two columns were utilised: an Acclaim

717   PepMap μ-precolumn cartridge 300 μm i.d. x 5 mm 5 μm 100 Å and an Acclaim

718   PepMap RSLC 75 μm x 15 cm 2 μm 100 Å (Thermo Scientific). The columns were

719   installed on an Ultimate 3000 RSLCnano system (Dionex). Mobile phase buffer A

720   was 0.1% aqueous formic acid and mobile phase B was composed of 100%

721   acetonitrile containing 0.1% formic acid. Samples were loaded onto the μ-precolumn

722   equilibrated in 50% aqueous acetonitrile containing 0.1% trifluoroacetic acid for 8

723   min at 10 μL min^{-1}. After which compounds were eluted onto the analytical column

724   following a 75 min gradient for which the mobile phase B concentration was

725   increased from 50% B to 80% over 15 min, then maintained at 80% B for 50 minutes,

726   then decreased to 50% over 1 min, followed by a 9 min wash at 50% B. Species were

727   analysed by electrospray ionisation mass spectrometry. Survey scans of precursors

728   from 150 to 1500 m/z were performed at 60K resolution (at 200 m/z) with a 4×10^5

729   ion count target. Tandem MS was performed by isolation at 1.6 Th with the

730   quadrupole, HCD fragmentation with normalised collision energy of 32, and rapid

731   scan MS analysis in the ion trap. The MS/MS ion count target was set to 2×10^5 and

732   the maximum injection time was 50 ms. A filter targeted inclusion mass list was used

733   to select the precursor ions.

734

735   <u>Data availability</u>

736   The tetronasin biosynthetic gene cluster sequence is available on GenBank under the

737   accession number: FJ462704. Crystal structure data is available on the PDB database

738   under the accession numbers: 6NOI (Tsn15) & 6NNW (Tsn15-substrate complex).

739   All other data that supports the findings of this study is available from the

740   corresponding author upon reasonable request.

752   Author contributions

753   R.L., P.F.L., F.J.L., M.T. and M.V.B.D. developed the hypothesis and designed the

754   study. Y.D., Y.S., and M.S. cloned, sequenced and analyzed gene clusters; R.L., Y.S.,

755   H.H., carried out gene deletions, M.T. and R.J. carried out and analysed experiments

756   with chain-terminating probes; R.L. carried out protein expression and purification, *in*

757   *vitro* experiments and compound isolation; R.L. and F.J.L. performed compound

758   characterisation. F.C.R.P., R.L. and M.V.B.D. solved crystal structures. All authors

759   analysed and discussed the results. P.F.L., R.L., and F.C.R.P. prepared the manuscript.

760   Competing Interests

761   The authors declare no competing interests
762   **References:**

763   1. Diels, O. & Alder, K. Synthesen in der hydroaromatischen Reihe. *Justus Liebigs*

764   *Annalen der Chemie* **460**, 98–122 (1928).

765   2. Corey, E. J. Catalytic Enantioselective Diels-Alder reactions: Methods,

766   Mechanistic Fundamentals, Pathways, and Applications. *Angew. Chem. Int. Ed.*

767   *Engl.* **41**, 1650–1667 (2002).

768   3. Lichman, B. R., O'Connor, S. E. & Kries, H. Biocatalytic Strategies Towards [4+

769   2] Cycloadditions. *Chem. Eur. J.* **25**, 6864-6877 (2019).

770   4. Jeon, B., Wang, S.-A., Ruszczycky, M. W. & Liu, H. Natural [4 + 2]-Cyclases.

771   *Chem. Rev.* **117**, 5367–5388 (2017).

772   5. Ma, S. M. *et al.* Complete Reconstitution of a Highly Reducing Iterative

773   Polyketide Synthase. *Science* **326**, 589–592 (2009).

774   6. Kasahara, K. *et al.* Solanapyrone Synthase, a Possible Diels–Alderase and

775   Iterative Type I Polyketide Synthase Encoded in a Biosynthetic Gene Cluster

776   from *Alternaria solani*. *ChemBioChem* **11**, 1245–1252 (2010).

777   7. Kim, H. J., Ruszczycky, M. W., Choi, S., Liu, Y. & Liu, H. Enzyme-catalysed

778   [4+2] Cycloaddition is a Key Step in the Biosynthesis of Spinosyn A. *Nature* **473**,

779   109–112 (2011).

780   8. Fage, C. D. *et al.* The Structure of SpnF, a Standalone Enzyme that Catalyzes

781   [4+2] Cycloaddition. *Nat. Chem. Biol.* **11**, 256–258 (2015).

782   9. Hashimoto, T. *et al.* Biosynthesis of Versipelostatin: Identification of an Enzyme-

783   Catalyzed [4+2]-Cycloaddition Required for Macrocyclization of Spirotetronate-

784   Containing Polyketides. *J. Am. Chem. Soc.* **137**, 572–575 (2015).

785   10. Byrne, M. J. *et al.* The Catalytic Mechanism of a Natural Diels–Alderase

786   Revealed in Molecular Detail. *J. Am. Chem. Soc.* **138**, 6095-6098 (2016).

787 11. Tian, Z. *et al.* An Enzymatic [4+2] Cyclization Cascade Creates the Pentacyclic

788   Core of Pyrroindomycins. *Nat. Chem. Biol.* **11**, 259–265 (2015).

789 12. Zhang, Z. *et al.* Enzyme-Catalyzed Inverse-Electron Demand Diels–Alder

790   Reaction in the Biosynthesis of Antifungal Ilicicolin H. *J. Am. Chem. Soc.* **141**,

791   5659–5663 (2019).

792 13. Cogan, D. P. *et al.* Structural Insights into Enzymatic [4+2] *aza*-Cycloaddition in

793   Thiopeptide Antibiotic Biosynthesis. *Proc. Natl. Acad. Sci.* **114**, 12928–12933

794   (2017).

795 14. Ohashi, M. *et al.* SAM-dependent Enzyme-Catalysed Pericyclic Reactions in

796   Natural Product Biosynthesis. *Nature* **549**, 502–506 (2017).

797 15. Demetriadou, A. K. *et al.* Biosynthesis of the Polyketide Polyether Antibiotic ICI

798   139603 in *Streptomyces longisporoflavus* from ^{18}O-labelled Acetate and

799   Propionate. *J. Chem. Soc., Chem. Commun.* **19**, 408–410 (1985).

800 16. Demydchuk, Y. *et al.* Analysis of the Tetronomycin Gene Cluster: Insights into

801   the Biosynthesis of a Polyether Tetronate Antibiotic. *ChemBioChem* **9**, 1136–

802   1145 (2008).

803 17. Sun, Y., Hong, H., Gillies, F., Spencer, J. B. & Leadlay, P. F. Glyceryl-S-Acyl

804   Carrier Protein as an Intermediate in the Biosynthesis of Tetronate Antibiotics.

805   *ChemBioChem* **9**, 150–156 (2008).

806 18. Hailes, H. C., Jackson, C. M., Leadlay, P. F., Ley, S. V. & Staunton, J.

807   Biosynthesis of Tetronasin: Part 1 Introduction and Investigation of the Diketide

808   and Triketide Intermediates Bound to the Polyketide Synthase. *Tetrahedron Lett.*

809   **35**, 307–310 (1994).

810 19. Boons, G.-J. *et al.* Novel Polyene Cyclisation Routes to the Acyl Tetronic Acid

811   Ionophore Tetronasin (ICI M139603). *Tetrahedron Lett.* **35**, 323–326 (1994).

812   20. Riva, E. *et al.* Chemical Probes for the Functionalization of Polyketide

813   Intermediates. *Angew. Chem. Int. Ed.* **53**, 11944–11949 (2014).

814   21. Tosin, M., Smith, L. & Leadlay, P. F. Insights into Lasalocid A Ring Formation

815   by Chemical Chain Termination *in vivo*. *Angew. Chem. Int. Ed. Engl.* **50**, 11930–

816   11933 (2011).

817   22. Zheng, Q. *et al.* Structural Insights into a Flavin-Dependent [4+2] Cyclase that

818   Catalyzes *trans*-Decalin Formation in Pyrroindomycin Biosynthesis. *Cell Chem.*

819   *Biol.* **25**, 718-727 (2018).

820   23. Bosserman, M. A., Downey, T., Noinaj, N., Buchanan, S. K. & Rohr, J.

821   Molecular Insight into Substrate Recognition and Catalysis of Baeyer–Villiger

822   Monooxygenase MtmOIV, the Key Frame-Modifying Enzyme in the

823   Biosynthesis of Anticancer Agent Mithramycin. *ACS Chem. Biol.* **8**, 2466–2477

824   (2013).

825   24. Vieweg, L., Reichau, S., Schobert, R., Leadlay, P. F. & Süssmuth, R. D. Recent

826   Advances in the Field of Bioactive Tetronates. *Nat. Prod. Rep.* **31**, 1554–1584

827   (2014).

828   25. Jiang, X. & Wang, R. Recent Developments in Catalytic Asymmetric Inverse-

829   Electron-Demand Diels–Alder Reaction. *Chem. Rev.* **113**, 5515–5546 (2013).

830   26. Pałasz, A. Recent Advances in Inverse-Electron-Demand Hetero-Diels–Alder

831   Reactions of 1-*oxa*-1,3-Butadienes. *Top. Curr. Chem (Cham).* **374**, 24 (2016).

832   27. Zheng, Q. *et al.* Enzyme-Dependent [4+2] Cycloaddition Depends on Lid-like

833   Interaction of the N-Terminal Sequence with the Catalytic Core in PyrI4. *Cell*

834   *Chemical Biology* **23**, 352–360 (2016).

835   28. Hofmann, E., Zerbe, P. & Schaller, F. The Crystal Structure of *Arabidopsis*

836   *thaliana* Allene Oxide Cyclase: Insights into the Oxylipin Cyclization Reaction.

837   *Plant Cell* **18**, 3201–3217 (2006).

838   29. Yoeun, S., Cho, K. & Han, O. Structural Evidence for the Substrate Channeling of

839   Rice Allene Oxide Cyclase in Biologically Analogous Nazarov Reaction. *Front.*

840   *Chem.* **6**, 500 (2018) DOI: 10.3389/fchem.2018.00500.

841   30. Costa, K. C., Glasser, N. R., Conway, S. J. & Newman, D. K. Pyocyanin

842   Degradation by a Tautomerizing Demethylase Inhibits *Pseudomonas aeruginosa*

843   Biofilms. *Science* **355**, 170–173 (2017).

844   31. Wilkinson, C. J. *et al.* Increasing the Efficiency of Heterologous Promoters in

845   Actinomycetes. *J. Mol. Microbiol. Biotechnol.* **4**, 417–426 (2002).

846   32. Harding S. E., Rowe S. E. *Analytical Ultracentrifugation in Biochemistry and*

847   *Polymer Science*. Royal Society of Chemistry: Cambridge (United Kingdom),

848   (1992).

849   33. Kabsch, W. XDS. *Acta Crystallogr. D Biol. Crystallogr.* **66**, 125–132 (2010).

850   34. Evans, P. R. & Murshudov, G. N. How Good are my Data and what is the

851   Resolution? *Acta Crystallogr. D Biol. Crystallogr.* **69**, 1204–1214 (2013).

852   35. Winn, M. D. *et al.* Overview of the CCP4 Suite and Current Developments. *Acta*

853   *Crystallogr. D Biol. Crystallogr.* **67**, 235–242 (2011).

854   36. Terwilliger, T. C. *et al.* Decision-Making in Structure Solution using Bayesian

855   Estimates of Map Quality: the PHENIX AutoSol Wizard. *Acta Crystallogr. D*

856   *Biol. Crystallogr.* **65**, 582–601 (2009).

857   37. Adams, P. D. *et al.* The Phenix Software for Automated Determination of

858   Macromolecular Structures. *Methods* **55**, 94–106 (2011).

859   38. Terwilliger, T. C. *et al.* Iterative Model Building, Structure Refinement and

860   Density Modification with the PHENIX AutoBuild Wizard. *Acta Crystallogr. D*

861   *Biol. Crystallogr.* **64**, 61–69 (2008).

862   39. McCoy, A. J. Solving Structures of Protein Complexes by Molecular

863   Replacement with Phaser. *Acta Crystallogr. D Biol. Crystallogr.* **63**, 32–41

864   (2007).

865   40. Afonine, P. V. *et al.* Towards Automated Crystallographic Structure Refinement

866   with phenix.refine. *Acta Crystallogr. D Biol. Crystallogr.* **68**, 352–367 (2012).

867   41. Emsley, P. & Cowtan, K. Coot: Model-Building Tools for Molecular Graphics.

868   *Acta Crystallogr. D Biol. Crystallogr.* **60**, 2126–2132 (2004).

869   42. Chen, V. B. *et al.* MolProbity: All-Atom Structure Validation for Macromolecular

870   Crystallography. *Acta Crystallogr. D Biol. Crystallogr.* **66**, 12–21 (2010).

871   43. Gibson, D. G. *et al.* Enzymatic Assembly of DNA Molecules up to Several

872   Hundred Kilobases. *Nat. Methods* **6**, 343–345 (2009).

873   44. MacNeil, D. J. *et al.* Analysis of *Streptomyces avermitilis* Genes Required for

874   Avermectin Biosynthesis Utilizing a Novel Integration Vector. *Gene* **111**, 61–68

875   (1992).

876   45. Sievers, F. *et al.* Fast, Scalable Generation of High‑Quality Protein Multiple

877   Sequence Alignments using Clustal Omega. *Mol. Syst. Biol.* **7**, 539 (2011).

878   46. Laskowski, R. A. *et al.* PDBsum: a Web-Based Database of Summaries and

879   Analyses of all PDB Structures. *Trends Biochem. Sci.* **22**, 488–490 (1997).

880   47. Tian, W., Chen, C., Lei, X., Zhao, J. & Liang, J. CASTp 3.0: Computed Atlas of

881   Surface Topography of Proteins. *Nucleic Acids Res.* **46**, 363–367 (2018).

882   48. Bulsing, J. M. *et al.* Biosynthesis of the Polyketide Antibiotic ICI139603 in

883   *Streptomyces longisporoflavus*: Assignment of the ^{13}C NMR Spectrum by Two-

884   Dimensional Methods, and Determination of the Origin of the Carbon Atoms. *J.*

885   *Chem. Soc., Chem. Commun.* **19**, 1301–1302 (1984).

886   49. Gelin, S. & Pollet, P. Tautomerism in Acyl Tetronic Acids. *Tetrahedron Lett.* **21**,

887   4 (1980).

888
889
890

891

892

893

894

895

896

897

898

899

900

901

902

903

904

905

906

907

908
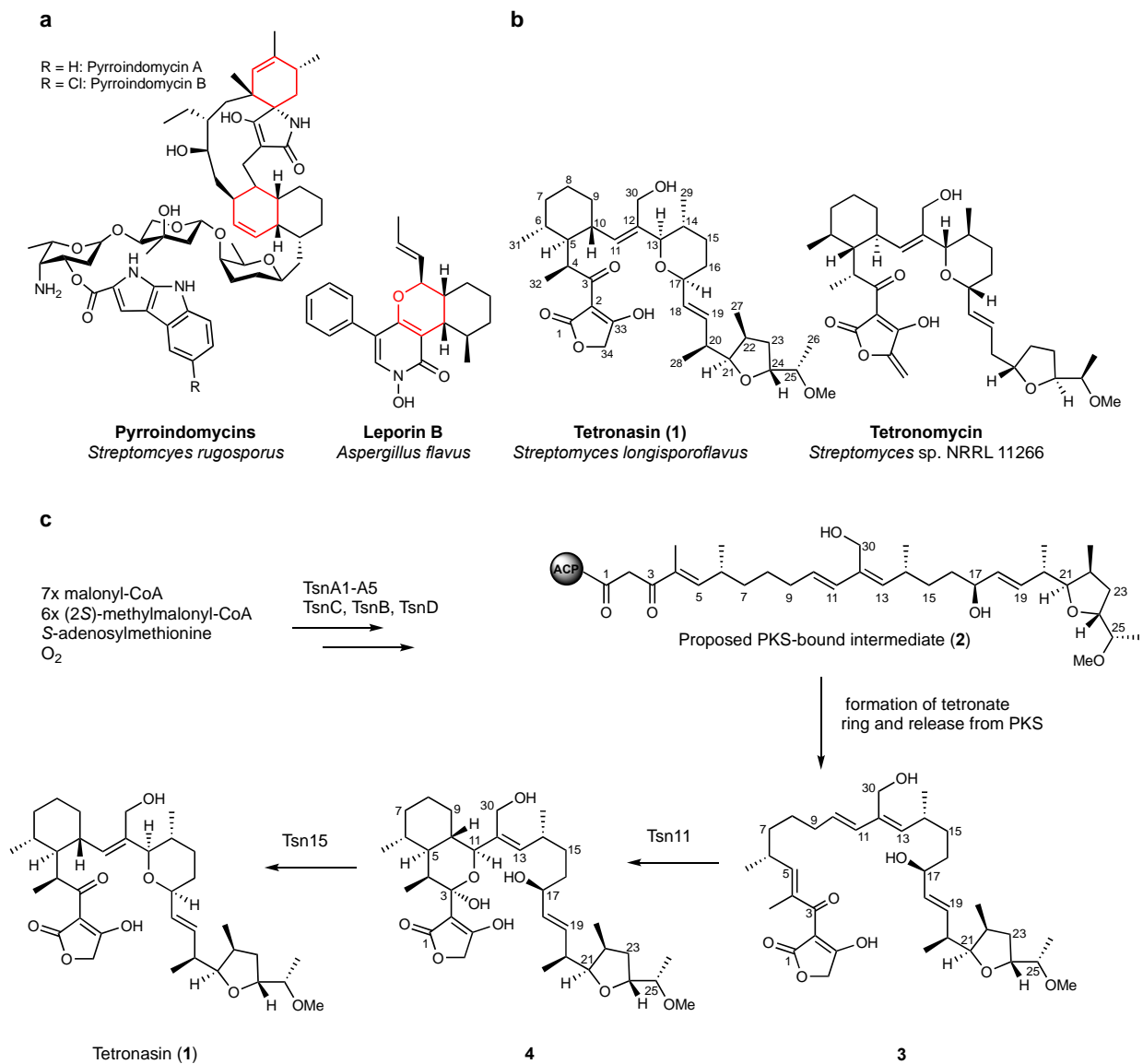
909

910
911
912
913
914
915
916

917
918

Figure 1. [4+2] cyclases in polyether tetronate biosynthesis. a, Structures of pyrroindomycin and leporin B, two polyketide natural products that require a [4+2] cyclase in their biosynthesis to create the rings highlighted in red. **b**, Structures of the polyether tetronate antibiotics tetronasin (**1**) and tetronomycin. **c**, Proposed role of the [4+2] cyclase homologues Tsn11 and Tsn15 in tetronasin biosynthesis.
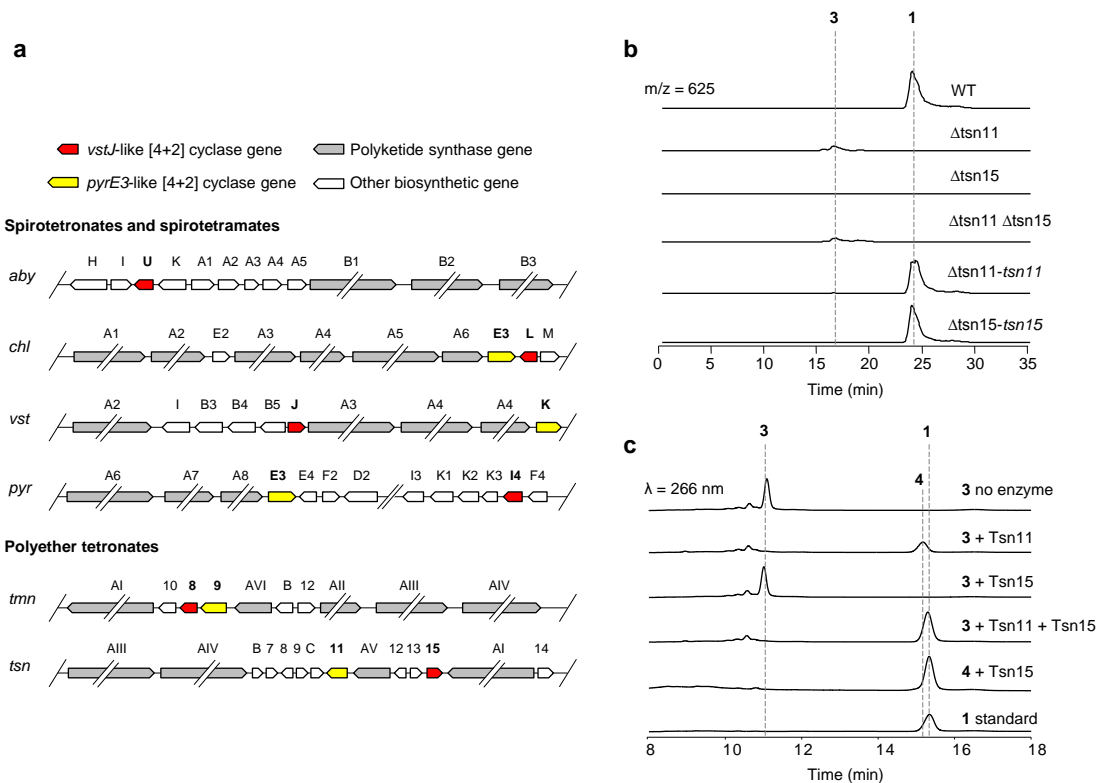
Figure 2. Functional characterisation of the Diels-Alderase homologues Tsn11 and Tsn15 in tetronasin biosynthesis. a, The biosynthetic gene clusters of tetronomycin (*tmn*) and tetronasin (*tsn*) encode a VstJ-like (red) and PyrE3-like (yellow) [4+2] cyclase characteristic of spirotetronate and spirotetramate biosynthesis pathways including abyssomicin (*aby*), chlorothricin (*chl*), veripelostatin (*vst*), and pyrroindomycin (*pyr*). Only partial biosynthetic gene clusters are displayed and individual genes are not shown to scale. **b,** HPLC-MS analysis of the production of tetronasin **1** (m/z = 625) and intermediate **3** (m/z = 625) from wildtype *S. longisporoflavus*, *S. longisporoflavus* Δtsn11, Δtsn15, and Δtsn11 Δtsn15, gene deletion mutants, and genetically complemented *S. longisporoflavus* deletion mutants. Data are representative of three independent experiments. **c,** HPLC analysis of the *in vitro* conversion of intermediate **3** into tetronasin **1** using purified Tsn11 and Tsn15. Data are representative of three independent experiments.
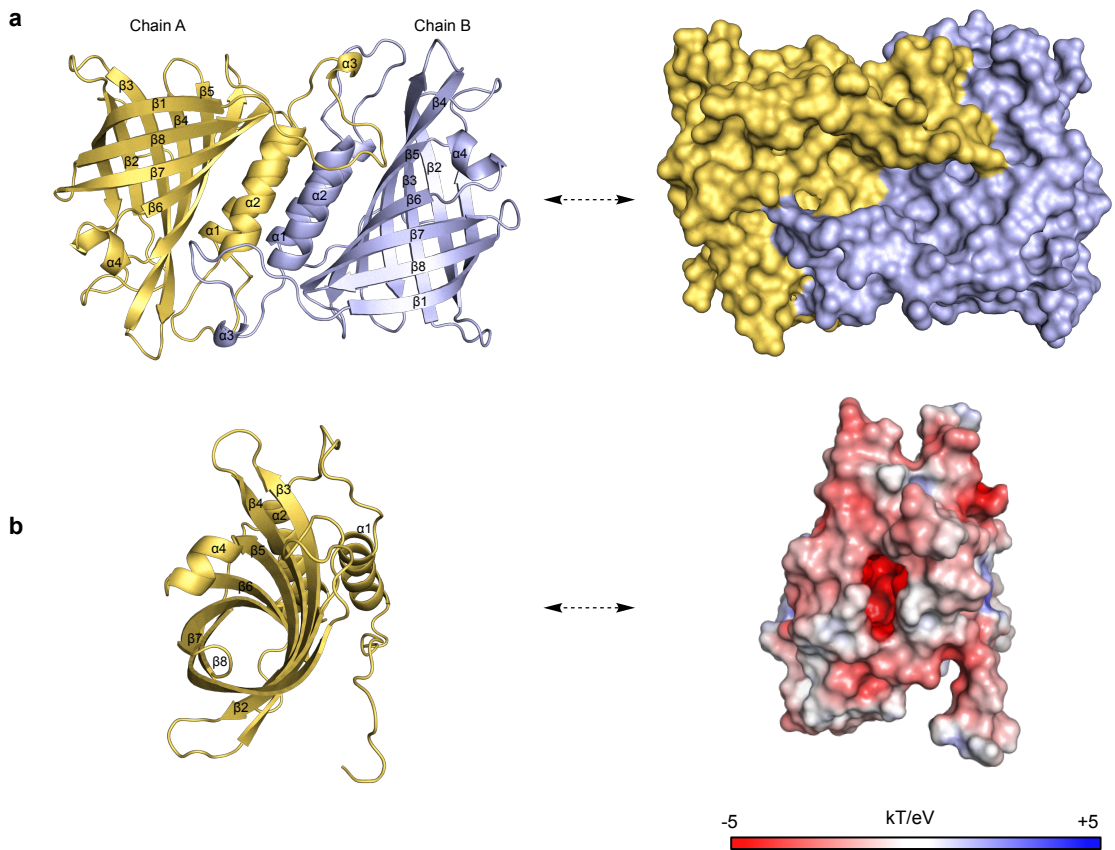
Figure 3. Crystal structure of Tsn15. The crystal structure of Tsn15 was solved to 1.8 Å resolution using SAD phasing. **a,** Ribbon and surface representation of the homodimeric Tsn15. **b.** The active-site cavity within the β-barrel of Tsn15. Right: surface charge representation contoured at ±5 kT/eV; blue/red.
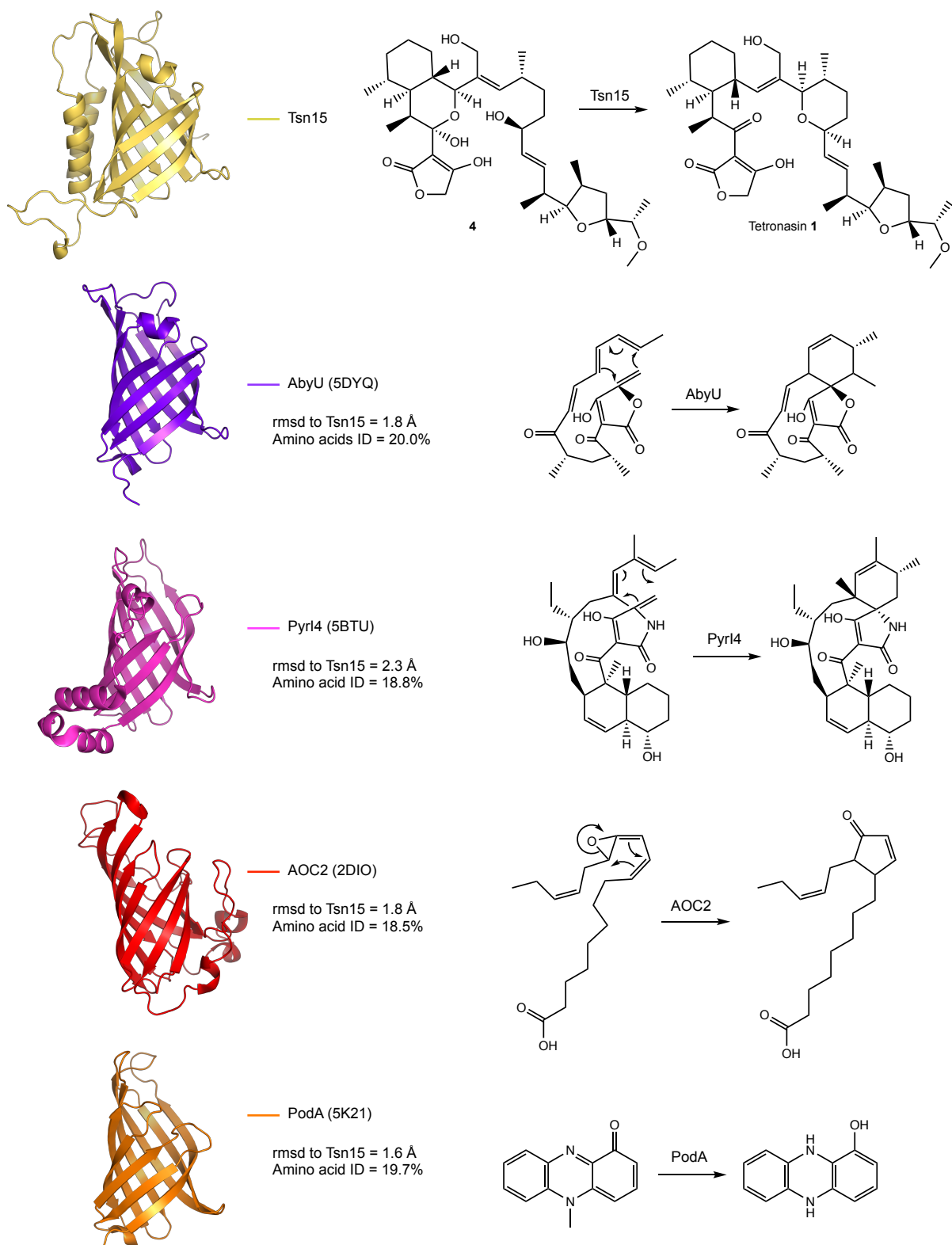
Figure 4 – Structural homologues of Tsn15 and their respective reactions. The Cα chain of Tsn15 was aligned with its structural homologues AbyU, PyrI4, AOC2, and PodA. Beside each structure is its rmsd value to Tsn15, amino acid identity (%) to Tsn15, and the reaction it catalyses.
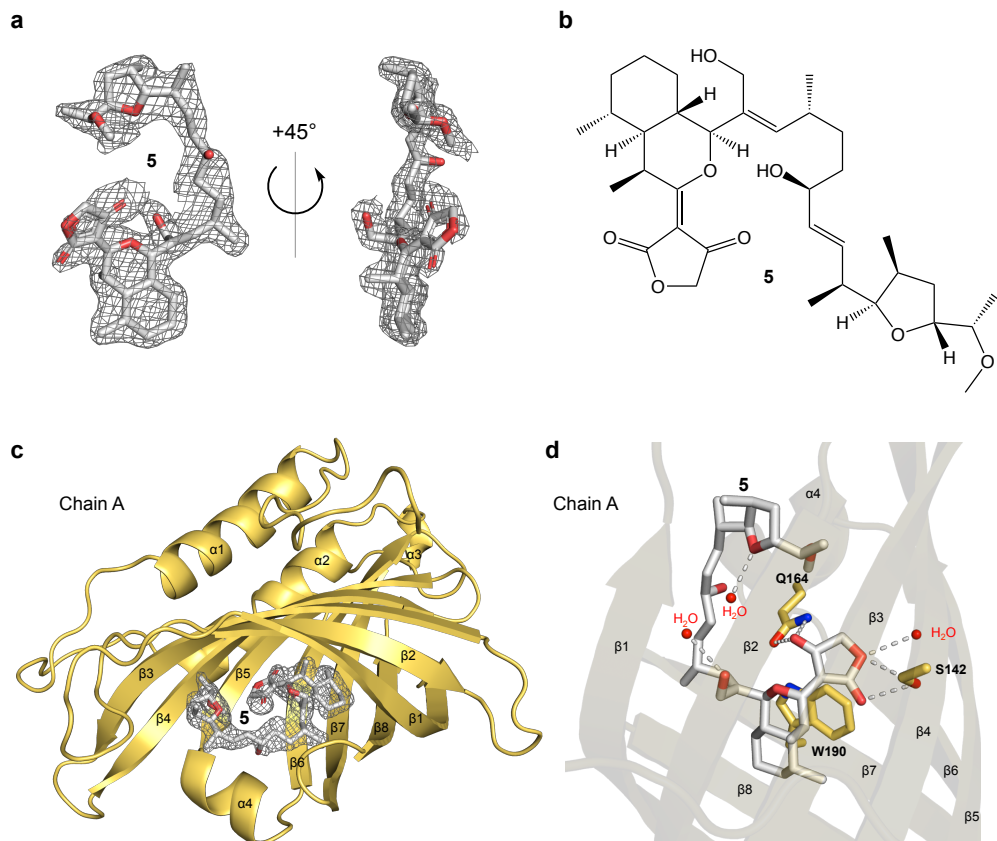
Fig. 5. Structure of Tsn15 and a Tsn15-substrate complex.
a, F_o-F_c of **5** (contoured to 2.0 σ) and its chemical structure. **b,** Tsn15 in complex with intermediate **5**. The F_o-F_c map of **5** could be clearly assigned in the β-barrel cavity of Tsn15 chain A. Contouring to 2.0 σ. **c,** The detailed binding interactions between intermediate **5** and the internal β-barrel residues of Tsn15 (chain A) are shown. The dotted grey lines represent hydrogen bonding.
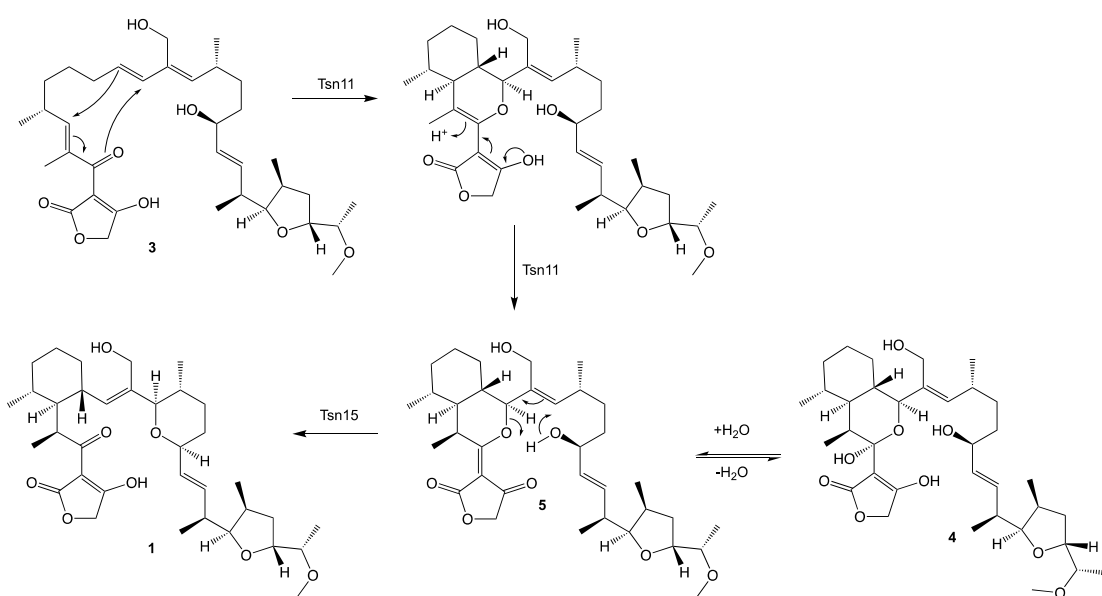
Fig. 6. Proposed mechanism for formation of the cyclohexane and tetrahydropyran rings of tetronasin. Tsn11 catalyses an inverse-electron-demand hetero-Diels-Alder reaction to form an oxadecalin intermediate. The oxadecalin is hydrated to form the cyclic hemiacetal **4** which was purified from the Tsn11 + **3** assay and structurally characterised. Tsn15 then catalyses dehydration of **4** to form **5** (which crystallised in the active site of Tsn15), followed by a pericyclic rearrangement to form the tetrahydropyran ring and fragment the oxadecalin, producing tetronasin **1**.

Tetronasin biosynthetic gene cluster

tsn11   *tsn15*

[4+2] cyclase homologues

i*n vitro* reconstitution of cyclohexane and tetrahydropyran biosynthesis

Tsn11

Tsn15

Open ring intermediate   Oxadecalin intermediate   **Tetronasin**
Streptomyces longisporoflavus